Revised version 4/29/22

# Comparison between Ab Initio Molecular Dynamics and OPLS-based Force Fields for Ionic Liquid Solvent Organization

**Kun Yue, Brian Doherty, and Orlando Acevedo***

*Department of Chemistry, University of Miami, Coral Gables, Florida 33146*

*E-mail: orlando.acevedo@miami.edu*

*Submitted March 8, 2022*

**Abstract:** OPLS-based force fields (FFs) have been shown to provide accurate bulk phase properties for a wide variety of imidazolium-based ionic liquids (ILs). However, the ability of OPLS to reproduce IL solvent structure is not as well validated given a relative lack of high-level theoretical or experimental data available for comparison. In this study, *ab initio* molecular dynamics (AIMD) simulations were performed for three widely used ionic liquids: the 1-butyl-3-methylimidazolium cation with chloride, tetrafluoroborate, or hexafluorophosphate anions, i.e., [BMIM][Cl], [BMIM][$BF_4$], and [BMIM][$PF_6$], respectively, as a basis for further assessment of two unique IL FFs: the ±0.8 charge-scaled OPLS-2009IL and the OPLS-VSIL. The OPLS-2009IL FF employs a traditional all-atom functional form, whereas the OPLS-VSIL was developed using a virtual site that offloads negative charge to inside the plane of the ring with careful attention given to reproducing hydrogen bonding. Detailed comparisons between AIMD and the OPLS FFs were made based on radial distribution functions (RDFs), combined distribution functions (CDFs), and spatial distribution functions (SDFs) to examine cation-anion interactions and $\pi^+$-$\pi^+$ stacking between the imidazolium rings. While both FFs were able to correctly capture the general solvent structure of these popular ILs, the OPLS-VSIL quantitatively reproduced interaction distances more accurately. In addition, this work provides further insight into the different short- and long-range structure patterns of these popular ionic liquids.

## Introduction

Ionic liquids (IL) are an exciting class of solvent with technological capabilities that extend far beyond solvating molecules.[1-8] These solvents are composed exclusively of ions that melt near room temperature and often possess large cations featuring an ionic head group and a nonpolar alkyl side-chain, e.g., 1-butyl-3-methylimidazolium [BMIM] (Scheme 1).[9-12] Delocalization of charge over several atoms and asymmetry in either the size or shape of the cation or anion are essential in the construction of these materials. The physical and chemical properties of ILs are fundamentally related to their solvent structure.[13, 14] Due to their extensive potential to alter physical and chemical behavior through functionalization, considerable effort has been put forth by the ionic liquid community to better understand the nature of these intermolecular interactions.[15-23]

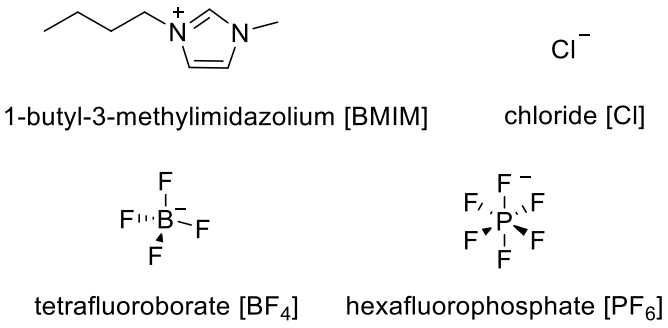


**Scheme 1.** Ionic liquid forming ions.

*Ab initio* molecular dynamics (AIMD) simulations have become an excellent tool in recent years for understanding the microscopic structure of ionic liquids.[24-31] AIMD describes the propagation of atoms through classical mechanics, but computes the forces 'on the fly' by using an electronic structure method, typically density functional theory (DFT) where the electronic orbitals are expanded in a plane-wave basis set.[32] AIMD calculations are ultimately limited by the

accuracy of the DFT methods. Fortunately, a reported examination of multiple density functional approximations found several methods, e.g., revPBE and OLYP, provided a reliable description of ionic liquids.[33] The inclusion of dispersion-corrections, i.e., DFT-D3,[34] was determined to be necessary for accurate AIMD ionic liquid simulations.[33, 35, 36] For example, Kirchner and co-workers demonstrated that the addition of dispersion corrections to the AIMD simulation of 1-ethyl-3-methylimidazolium thiocyanate, [EMIM][SCN], had little effect on the RDFs, but did appreciably enhance $\pi^+$-$\pi^+$ stacking between the imidazolium cations.[29] Additional AIMD-based studies by Kirchner provided a detailed examination of IL interactions in water,[25, 37-40] gave further insight into the unique properties of chloroaluminate-based ILs,[41] and explored the effect of chain lengths in protic ILs.[42]

The high computational cost of AIMD often limits simulations to short timescales of ~100 ps and a reduced simulation box size composed of 32 ion pairs that prohibits description of the medium-long structural order present in ionic liquids.[43, 44] This speaks to the present need of highly-accurate atomic-level ionic liquid force fields (FFs).[45-52] Our group published a nonpolarizable OPLS-based ionic liquid force field in 2009 (i.e., OPLS-2009IL),[53] which was reevaluated in 2017 using a new charge scaling of ±0.8 e to mimic polarization and charge transfer effects.[54] The scaled parameters yielded excellent agreement with experimental densities, heats of vaporization ($\Delta H_{vap}$), viscosities, diffusion coefficients, heat capacities, surface tensions, and other relevant solvent data. However, many existing IL force fields including OPLS-2009IL have potential shortcomings, such the over- or underestimation of hydrogen-bonding strength and errors in solvent interactions/organization. This led our group to undertake a new parameterization effort for imidazolium-based ILs that featured a novel topology that incorporated a virtual site bisecting the nitrogen atoms that offloads negative charge to inside the plane of the ring. This new force

field (called OPLS-VSIL) included empirical charges guided by free energy of hydration calculations and new Lennard-Jones terms that were fine-tuned for the 1-alkyl-3-methylimidazolium cations and 11 different anions.[55] The OPLS-VSIL gave quantitative reproduction of experimental data in many cases for bulk-phase solvent properties[56] and reproduced radial distribution functions (RDFs) derived from reported AIMD simulations and experiments.

While multiple AIMD ionic liquid simulations have been published (by Kirchner in particular), three of the most widely used solvents in experimental literature, i.e., 1-butyl-3-methylimidazolium cation with chloride, tetrafluoroborate, and hexafluorophosphate anions, or [BMIM][Cl], [BMIM][$BF_4$], and [BMIM][$PF_6$], respectively, were not available in binary compositions during our FF developmental work. In this study, new AIMD simulations were performed for these three ionic liquids to examine cation-anion interactions and $\pi^+$-$\pi^+$ stacking between the imidazolium rings. A detailed comparison was made to results generated using both the OPLS-VSIL and OPLS-2009IL FFs. Radial, angular, and spatial distribution functions were used to further analyze the solvents and additional insight is provided into the different short- and long-range structure patterns of these ionic liquids.

**Computational Methods**

**AIMD Simulations.** Ab initio molecular dynamics simulations of 32 ion pairs were carried out using the CP2K program[57] (version 6.1) via the QUICKSTEP module at a DFT approximation level.[58] Periodic boundary conditions were applied to a cubic box with a length of 20.48 Å per side to reproduce the experimental density of 1.08 g/cm$^3$ for [BMIM][Cl], 21.55 Å to reproduce 1.20 g/cm$^3$ for [BMIM][$BF_4$], and 22.25 Å to reproduce 1.37 g/cm$^3$ for [BMIM][$PF_6$], at 25 ºC.[59, 60] The initial ion coordinates for the simulation box were constructed using the Packmol program.[61] The

electronic structure method employed was the revPBE functional[62] with Grimme's empirical D3 dispersion correction,[34, 63] as it provided accurate results for a prior AIMD simulation of an ionic liquid mixture composed of [BMIM], [Cl], and [$BF_4$].[25] The molecularly optimized double-ζ basis set (MOLOPT-DZVP-SR-GTH)[64] and the corresponding PBE Goedecker-Teter-Hutter pseudopotentials[65-67] for core electrons was applied to all atoms. A density CUTOFF criterion of 400 Ry was the utilized with the finest grid level, along with multigrids number 5 (NGRID 5 and REL_CUTOFF 60) using the smoothing for the electron density (NN10_SMOOTH) and its derivative (NN10).[58] The target accuracy threshold for the self-consistent field (SCF) convergence was changed to $1.0 \times 10^{-6}$. The use of the DIIS minimizer allowed for a faster orbital transformation (OT) through direct inversion in the iterative subspace. A maximum of 100 SCF iterations were performed per iteration, whereas a maximum of 10 iterations was completed for outer SCF loops. The PS extrapolation strategy was chosen for the wavefunction during MD with a high-precision convergence (EPS_DEFAULT of $1.0 \times 10^{-12}$).

The AIMD simulation was performed at 298.15 K in the canonical (NVT) ensemble using a Nosé-Hoover chain thermostat with a 50-fs time constant of the thermostat chain. Prior to the MD simulation, a geometry optimization was carried out with the convergence criterions for the maximum geometry change (MAX_DR) and the root mean square geometry change (RMS_DR) both set to $1.0 \times 10^{-3}$. An equilibration was carried out over 5 ps with the keyword REGION MASSIVE, i.e., a thermostat is individually applied for every degree of freedom of every single atom to achieve a faster equilibration. Following this initial equilibration, this keyword was replaced by GLOBAL and a second equilibration was performed for 30 ps. A production run was performed for 70 ps with a time step of 0.5 fs. Evaluation of the conserved quantity (total energy) gave a small percentage change over the total simulation, i.e., 0.029% for [BMIM][$PF_6$], 0.033%

for [BMIM][$BF_4$], and 0.04% for [BMIM][Cl]. Radial, combined, and spatial distribution functions were computed using the TRAVIS program[68] and plotted using Mathematica.

**OPLS-AA Force Field.** The OPLS-AA FF uses a combination of intramolecular and intermolecular terms to compute the total energy of the system.[69] The harmonic bond stretching and angle bending terms, the Fourier series for dihedral angles, and the intermolecular energies from Coulomb and 12-6 Lennard-Jones terms are provided in equations 1-4. The adjustable parameters are the force constants $k$, the $r_o$ and $\theta_o$ equilibrium bond and angle values, Fourier coefficients $V$, partial atomic charges, $q$, and Lennard-Jones radii and well-depths, σ and ε. All OPLS-2009IL and OPLS-VSIL ionic liquid parameters are available to download at https://github.com/orlandoacevedo/IL as preformatted GROMACS[70] files.

$$E_{bonds} = \sum_i k_{r,i}(r_i - r_{0,i})^2 \quad (1)$$

$$E_{angles} = \sum_i k_{\theta,i}(\theta_i - \theta_{0,i})^2 \quad (2)$$

$$E_{torsion} = \frac{1}{2}\sum_i [V_{1,i}(1 + cos\,\phi_i) + V_{2,i}(1 - cos\,2\phi_i) + V_{3,i}(1 + cos\,3\phi_i) + V_{4,i}(1 - cos\,4\phi_i)] \quad (3)$$

$$E_{nonbond} = \sum_i \sum_{j>i} \left\{ \frac{q_i q_j e^2}{r_{ij}} + 4\varepsilon_{ij} \left[ \left(\frac{\sigma_{ij}}{r_{ij}}\right)^{12} - \left(\frac{\sigma_{ij}}{r_{ij}}\right)^{6} \right] \right\} \quad (4)$$

Standard geometric combining rules, i.e., $\sigma_{ij} = (\sigma_{ii}\sigma_{jj})^{1/2}$ and $\varepsilon_{ij} = (\varepsilon_{ii}\varepsilon_{jj})^{1/2}$ were applied to the Lennard-Jones coefficients. Nonbonded interactions were calculated intermolecularly and for intramolecular atom pairs separated by three or more bonds. To apply the same parameters for both intra- and intermolecular interactions the 1,4-intramolecular interactions were reduced by a factor of 2.

**Molecular Dynamics.** Unbiased molecular dynamic (MD) simulations were carried out using the GROMACS 5.0.7 software package.[70] Cubic boxes containing 500 ion pairs were constructed with the Packmol program.[61] Periodic boundary conditions and Particle-Mesh Ewald summations were utilized. The systems were minimized using a steepest descent algorithm for 5000 steps. Equations of motion were integrated using the leap-frog algorithm with a time step of 1 fs. A temperature value of 298 K was kept constant using velocity rescaling with a stochastic term (v-rescale)[71] and a constant pressure of 1.0 bar was maintained with the Berendsen coupling during an isothermal-isobaric ensemble (NPT) simulation for 5 ns of equilibration. All covalent bonds to hydrogen atoms were constrained using the LINCS algorithm and a cutoff range for the short-range electrostatics was set to 13 Å. Production runs were performed for an additional 40 ns.

**Results and Discussion**

Simulations of three ionic liquids, i.e., [BMIM][$PF_6$], [BMIM][$BF_4$], and [BMIM][Cl], were performed using AIMD and the nonpolarizable OPLS-VSIL and 0.8*OPLS-2009IL FFs. Since reproduction of IL macroscopic bulk properties, e.g., densities, heats of vaporization, viscosities, diffusion coefficients, heat capacities, and surface tensions, was thoroughly investigated in our earlier parameterization efforts,[53-55] the focus of this work is to examine each FF's ability to replicate the microscopic intermolecular interactions predicted by the AIMD simulations. Radial distribution functions (RDFs), combined distribution functions (CDFs), and spatial distribution functions (SDFs) were used to examine cation-anion interactions and $\pi^+$-$\pi^+$ stacking between the imidazolium rings. Details for each individual IL investigated are provided below.

**[BMIM][$PF_6$].** Examining the [BMIM] cation to [$PF_6$] anion interaction through RDF plots found the computed shapes of the *g*(r) intensities and bond distances to be reasonably similar when comparing the OPLS-VSIL and 0.8*OPLS-2009IL FFs to AIMD (Figures 1 and S1). The intermolecular interaction involving the most acidic proton on the imidazolium ring, i.e., the H2 atom, with the P atom on the anion gave the largest peak height with *g*(r) values of 2.9-3.2 (Table 1). This interaction has been shown to play a major role in directing both local solvent organization and bulk properties.[72, 73] Perfect agreement was found in terms of the computed atomic separation of 328.3 pm between H2 and P for AIMD and OPLS-VSIL; however, the 0.8*OPLS-2009IL FF gave a longer H2−P distance of 358.3 pm (Table 1). Beyond the important H2 interaction, AIMD also found the other two ring hydrogen atoms (H4 and H5) gave a sizable *g*(r) peak height of 2.5 and a H4,5−P distance of 341.7 pm. Both OPLS FFs gave excellent agreement in terms of their peak intensity predictions compared to AIMD, but the OPLS-VSIL gave a slightly shorter bond distance (H4,5−P) of 335.0 pm, whereas 0.8*OPLS-2009IL yielded a longer distance of 361.7 pm. Upon exploration of potential hydrogen bonding interactions arising from the H atoms present on the alkyl side chains, the AIMD simulations found the methyl substituent H10 atoms and P gave a more intense peak value of 2.3 compared to a weaker value of 1.8 for the hydrogen atoms from the first carbon atom on the butyl side chain (H6). The OPLS-VSIL did a good job of reproducing these substituent H10 and H6 *g*(r) peak values at 2.4 and 1.9, respectively, but the 0.8*OPLS-2009IL gave more overestimated peak intensities of 2.6 and 2.2 (Table 1). Finally, the shapes in terms of *g*(r) and bond distances between P and the hydrogen atoms H7, H8, and H9 present on the butyl side chain were similar for AIMD and both FFs. Overall, both FFs provided a satisfactory reproduction of the AIMD-computed cation-anion RDF plots (Figure 1 and Table 1).

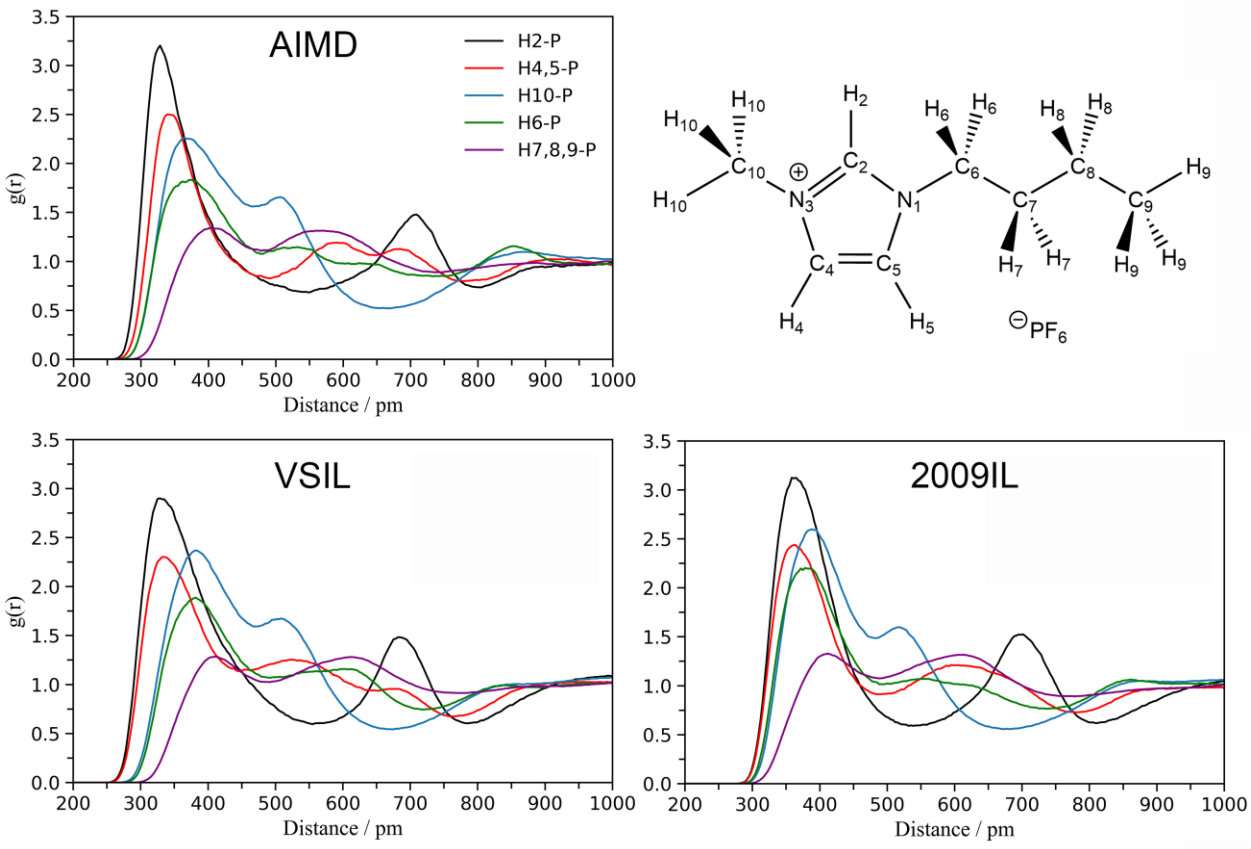


**Figure 1.** Computed radial distribution function plots between the hydrogen atoms of [BMIM] and the phosphorus atom of [$PF_6$] from AIMD, OPLS-VSIL, and 0.8*OPLS-2009IL simulations.

**Table 1.** Interaction Distances (pm) and *g*(r) from Radial Distribution Functions Computed using 0.8*OPLS-2009IL, OPLS-VSIL, and AIMD simulations for the Ionic Liquid [BMIM][$PF_6$].

| | distance (pm) | | | *g*(r) | | |
|---|---|---|---|---|---|---|
| Atoms[a] | 2009IL | VSIL | AIMD | 2009IL | VSIL | AIMD |
| H2-P | 358.3 | 328.3 | 328.3 | 3.1 | 2.9 | 3.2 |
| H4,5-P | 361.7 | 335.0 | 341.7 | 2.4 | 2.3 | 2.5 |
| H10-P | 388.3 | 381.7 | 365.0 | 2.6 | 2.4 | 2.3 |
| H6-P | 378.3 | 381.7 | 371.7 | 2.2 | 1.9 | 1.8 |

[a]See Figure 1 for atom definitions.

Combined distribution functions can provide additional information on the solvent structure by examining a specific distance, *d*, and angle, α, occurring between the cations and anions over the course of the simulation. For example, monitoring *d* and α between the crucial H2 atom of [BMIM] and the P atom of [$PF_6$] in the AIMD simulation found a particularly strong peak intensity (colored in red in Figure 2) located around *d* = 300-350 pm and α = 135-180°. The linear directionality of this hydrogen bond, e.g., donor-H···acceptor angle, suggests a strong interaction. However, it is important to point out that the intensity of the peaks are related to the number of neighbors and not the particular strength of a hydrogen bond, but one could infer their complementary relationship.[29] The OPLS-VSIL FF yielded a near identical CDF plot as compared to the AIMD simulation. However, the 0.8*OPLS-2009IL gave the strong H2-P intensity over a much broader angle range of α = 90-180° (Figure 2 in red color). This suggests that the 0.8*OPLS-2009IL may provide a less linear hydrogen bond and perhaps a slightly poorer reproduction of the [BMIM][$PF_6$] solvent organization. In addition, very intense peaks were predicted by 0.8*OPLS-2009IL at distances of *d* = 650-800 pm, which have significantly lower probabilities in the AIMD simulation. Additional CDF plots between the [BMIM] ring hydrogen atoms, H4 and H5, and the P atom yielded similar findings to the H2 plots (Figures S5 and S6).

An additional method for visualizing the preferential locations of the ions in the [BMIM][$PF_6$] simulations is the use of spatial distribution functions. These SDFs were built and analyzed using the TRAVIS program with an isosurface value of 7.00 particles/$nm^3$ for the anion region of [BMIM][$PF_6$] (colored in orange in Figure 3). The AIMD simulation found the anions preferred to occupy the area around the H2 hydrogen atom with additional interactions at the H4 and H5 locations. The AIMD and OPLS-VSIL gave similar SDF results (analogous to the CDF plots). In contrast, the 0.8*OPLS-2009IL SDF plots favored the "on-top" ion-ion interaction[74] and

lacked the more direct "in-plane" hydrogen bond interaction[75] computed in the other simulations. The 0.8*OPLS-2009IL findings are similar in performance to the charge scaled IL FF by Mondal and Balasubramanian[76] when examined using a nearest-neighbor approach.[77]

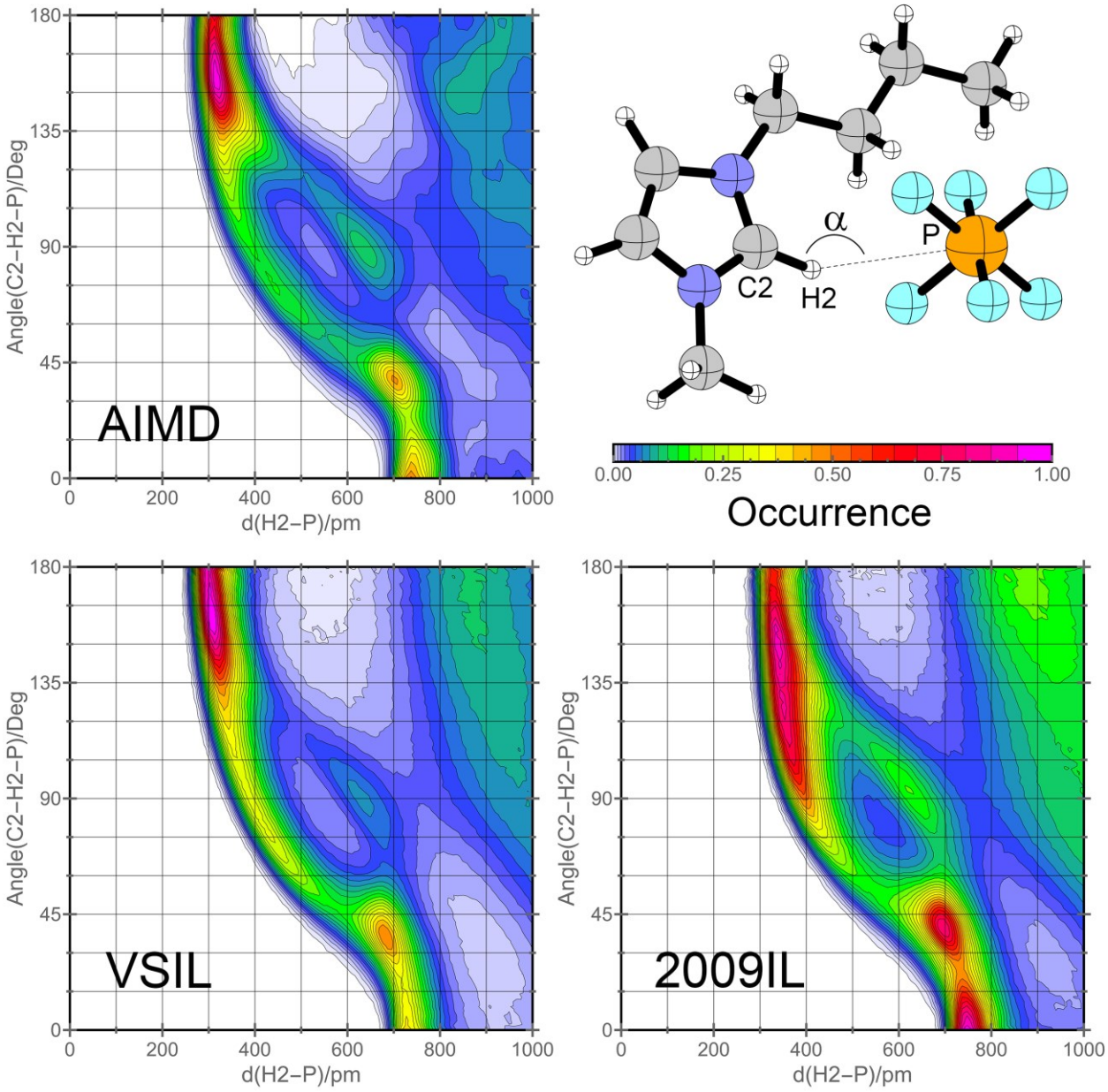


**Figure 2.** Combined distribution functions (CDFs) for the ionic liquid [BMIM][$PF_6$] from the AIMD, OPLS-VSIL, and 0.8*OPLS-2009IL simulations. Illustrations are given of the plotted

angle α versus the distance *d* between the H2 and P atoms. The CDF plot is given with a relative intensity color for the occurrence of the hydrogen bonding interaction.

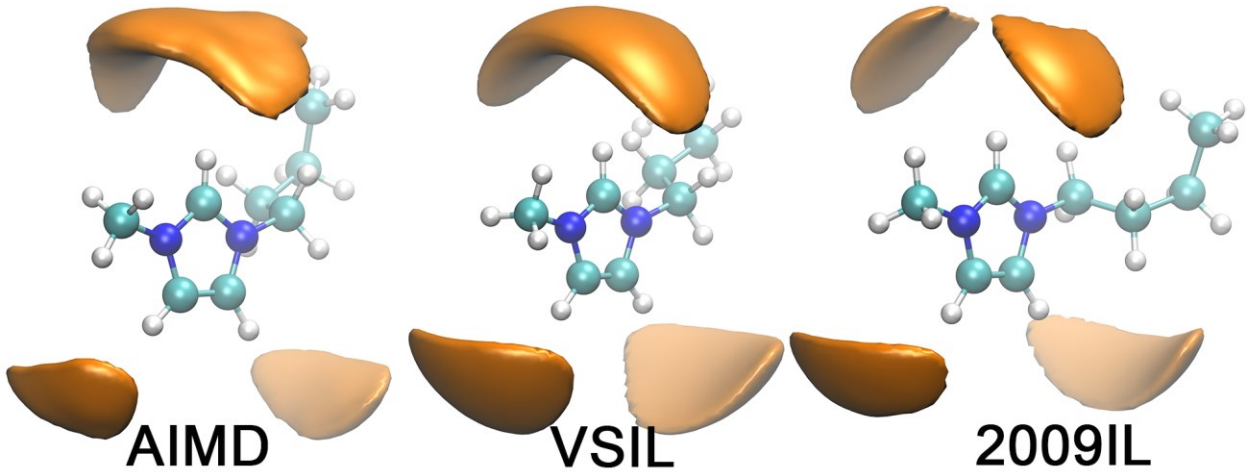


**Figure 3.** Spatial distribution function of the [$PF_6$] anion (orange color) around the [BMIM] cation in the ionic liquid simulation using AIMD, OPLS-VSIL, and 0.8*OPLS-2009IL simulations.

For additional structural examination of the [BMIM][$PF_6$] IL, the cation−cation interactions were explored by computing the orientation and frequency of any $\pi^+$-$\pi^+$ stacking present in the system. Previous theoretical calculations[78] and solid-state experimental X-ray studies[79] have shown that anion templated $\pi^+$-$\pi^+$ interactions are the major driving force in crystal packing. In addition, $\pi^+$-$\pi^+$ stacked motifs have also been identified in multiple crystal structures of imidazolium-based ILs.[80] The stabilization of these $\pi^+$-$\pi^+$ stacked clusters present in ILs is reportedly dominated by electrostatic interactions, although polarization, dispersion, and hydrogen bonding make appreciable contributions.[81-83] In this work, the center-of-ring (CoR) interaction between two [BMIM] cations were monitored using the angle, α, created by a normalized vector

(RN) perpendicular to the plane of the [BMIM] ring and the vector that connects two rings by their geometric centers as a function of distance, *d* (Figure 4). A typical equilibrium $d_{CoR\text{-}CoR}$ for two $\pi^+$-$\pi^+$ stacked [BMIM] rings has been reported as ~400 pm in IL combinations that featured 6 different anions.[84] However, the population of parallel stacked conformation, i.e., $\alpha$ near 0 and 180°, is dependent on the type of anion present. For example, $\pi^+$-$\pi^+$ preferential stacking has been reported for [BMIM] with $Br^-$, $I^-$, and acetate [OAc], but reduced stacking was found in the presence of fluorinated anions like trifluoroacetate [TFA] and bis(trifluoromethylsulfonyl)imide [$Tf_2N$].[84] Accordingly, the current AIMD simulations found the largest intensity peaks varied significantly according to distance (colored in red in Figure 4). For example, an intense population was computed at a *d* of around 400-500 pm at an $\alpha$ of approximately 0-30° (or 150-180°) and a second intense area was located at a *d* of 600-700 pm and an $\alpha$ of approximately 15-45° (or 135-160°). Overall, there were multiple $\pi^+$-$\pi^+$ interaction configurations present for [BMIM][$PF_6$] from the AIMD simulations, which may be indicative of the fluidity of conformations present in the solution phase. The 0.8*OPLS-2009IL and OPLS-VSIL all sampled within those regions, but the 0.8*OPLS-2009IL emphasized a larger population of $\pi^+$-$\pi^+$ parallel stacking at approximately 600 pm and 0° and 180°, whereas the OPLS-VSIL emphasized the region closer to 700 pm and 45° or 135°, which may be considered more of a slipped orientation (Figure 4). Given the emphasis of the virtual site to improve the H2-anion interaction in terms of cation-anion structural orientation, i.e., lie closer to the top of the ring for the larger anions, the consequence is that the stacking $\pi^+$-$\pi^+$ interaction is reduced. Further confirmed by the SDFs (Figure 3), the strong Columbic interactions present between the ions meant it was more probable for the anions to be orientated specifically towards the positively charged imidazolium hydrogen ring atoms (H2, H4, and H5 in Figure 1), which had a large influence on the subsequent positioning of the $\pi^+$-$\pi^+$ interaction.[77]

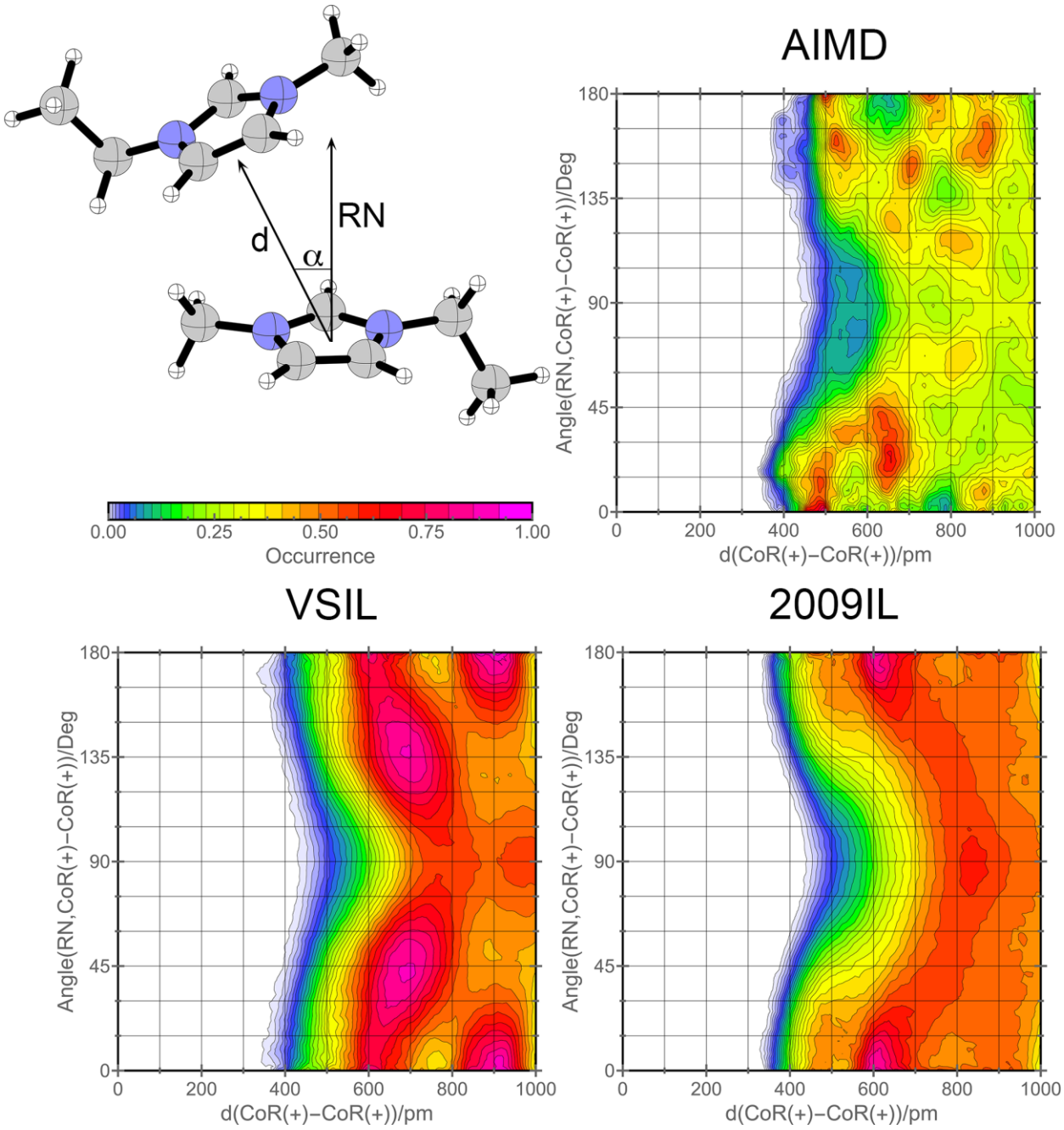


**Figure 4.** Combined distribution functions (CDFs) for the ionic liquid [BMIM][$PF_6$] from the OPLS-2009IL, OPLS-VSIL, and AIMD simulations. Illustrations are given of the plotted angle α versus the distance *d* for the center of the ring (CoR) interaction between two [BMIM]. The CDF plot is given with a relative intensity color for the CoR−CoR interactions. (Adapted with permission from *J. Phys. Chem. B* **2018**, *122*, 2962−2974. Copyright 2018 American Chemical Society).

Finally, the FF derived liquid structure of [BMIM][$PF_6$] was investigated by comparing RDFs and coordination numbers using the center-of-masses of the cations and anions. These RDFs provide the probability of finding an anion at a certain distance from a reference cation compared to the statistical average. Integration of the first peak yielded the number of anions located within the first solvation shell. The average coordination numbers ($N_{coord}$) and standard deviations were computed by splitting the MD trajectory into four parts. Table 2 compares the results from AIMD to both the 0.8*OPLS-2009IL and OPLS-VSIL FFs for all simulated ILs and found reasonable agreement between the maximum and minimum of the first peaks ($r_{max}$ and $r_{min}$) and $N_{coord}$. Figure S11 provides the center-of-mass RDF peak positions, heights, and shapes.

**Table 2.** Average Coordination Number ($N_{coord}$) and Positions (Å) of the First Maximum and Minimum in the Center-of-Mass RDFs between the BMIM cation and the Anions from AIMD, OPLS-VSIL, and 0.8*OPLS-2009IL simulations.

| | [BMIM][$PF_6$] | | | [BMIM][$BF_4$] | | | [BMIM][Cl] | | |
|---|---|---|---|---|---|---|---|---|---|
| | $r_{max}$ | $r_{min}$ | $N_{coord}$ | $r_{max}$ | $r_{min}$ | $N_{coord}$ | $r_{max}$ | $r_{min}$ | $N_{coord}$ |
| AIMD | 4.9 | 6.4 | 2.8 ± 0.1 | 4.7 | 6.0 | 2.2 ± 0.03 | 4.1 | 5.2 | 1.9 ± 0.2 |
| VSIL | 4.8 | 6.2 | 2.5 ± 0.1 | 4.5 | 5.9 | 2.4 ± 0.1 | 4.1 | 5.2 | 1.9 ± 0.1 |
| 2009IL | 5.0 | 6.6 | 2.9 ± 0.1 | 4.7 | 6.2 | 2.7 ± 0.1 | 4.3 | 5.4 | 2.1 ± 0.03 |

**[BMIM][$BF_4$].** Radial distribution analysis of the interaction between the [BMIM] cation and the [$BF_4$] anion found the H2−B interaction gave the largest *g*(r) peak with a value of 2.8 and a bond separation distance of 285.0 pm from the AIMD simulation (Figures 5 and S2, and Table 3). This most acidic hydrogen atom interaction was well reproduced by the OPLS-VSIL and 0.8*OPLS-2009IL FFs with *g*(r) peaks of 2.8 and 3.0, respectively. The OPLS-VSIL gave an excellent reproduction of the H2−B separation distance with a value of 291.7 pm; however, the

0.8*OPLS-2009IL did not perform as well with a larger separation of 331.7 pm (Table 3). A similar finding was found for the H4 and H5 ring hydrogen atoms where the sizable *g*(r) peak height of 2.4 computed using AIMD was well-reproduced with both FFs, but the AIMD-calculated H4,5−P distance of 301.7 pm was better modeled by the OPLS-VSIL FF with a computed distance of 295.0 pm (Table 3). The H10 and H6 atoms present on the methyl and butyl side chains, respectively, gave RDF *g*(r) peaks of 1.9 and 1.8 using AIMD that were better replicated by OPLS-VSIL, but the bond separations were overestimated by 10-40 pm (Table 3).

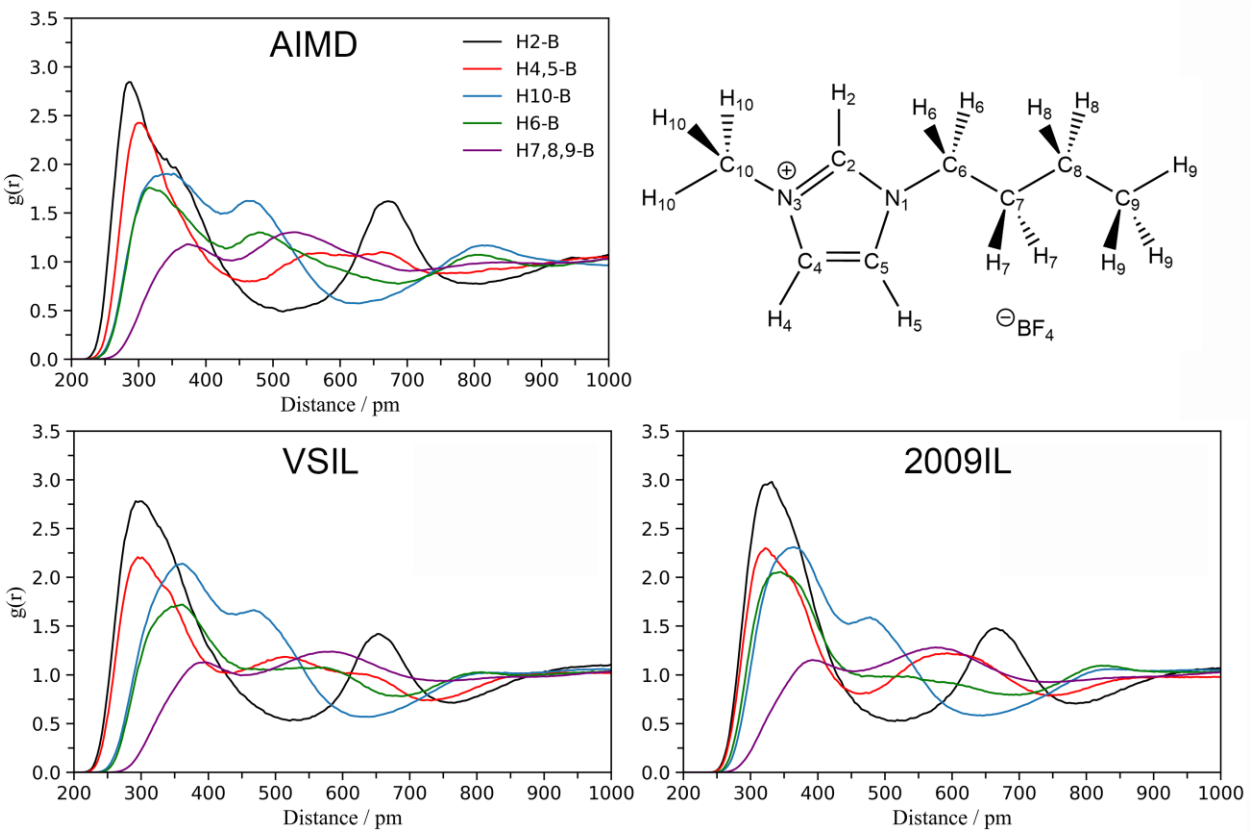


**Figure 5.** Computed radial distribution function plots between the hydrogen atoms of [BMIM] and the boron atom of [$BF_4$] from AIMD, OPLS-VSIL, and 0.8*OPLS-2009IL simulations.

**Table 3.** Interaction Distances (pm) and *g*(r) from Radial Distribution Functions Computed using 0.8*OPLS-2009IL, OPLS-VSIL, and AIMD simulations for the Ionic Liquid [BMIM][$BF_4$].

| | distance (pm) | | | *g*(r) | | |
|---|---|---|---|---|---|---|
| Atoms[a] | 2009IL | VSIL | AIMD | 2009IL | VSIL | AIMD |
| H2-B | 331.7 | 291.7 | 285.0 | 3.0 | 2.8 | 2.8 |
| H4,5-B | 321.7 | 295.0 | 301.7 | 2.3 | 2.2 | 2.4 |
| H10-B | 365.0 | 361.7 | 351.7 | 2.3 | 2.1 | 1.9 |
| H6-B | 345.0 | 361.7 | 315.0 | 2.1 | 1.7 | 1.8 |

[a]See Figure 5 for atom definitions.

Combined distribution functions were computed from the AIMD trajectory between the H2 atom of [BMIM] and the B atom of [$BF_4$] and an intense peak region was computed at $d$ = 250-300 pm and $\alpha$ = 135-180° (colored in red in Figure 6). OPLS-VSIL reproduced the AIMD distance and angle ranges well, whereas OPLS-2009IL found the maximum intensity peak at a longer $d$ of 300-350 pm and a wider-angle range of 90-180°. In general, the solvent organization of [BMIM][$BF_4$] was similar to [BMIM][$PF_6$], i.e., a linear donor-H···acceptor hydrogen bond angle and reduced interaction peak intensities at distances of 650-800 pm and angles of 30-45°. Additional CDF plots between the [BMIM] ring hydrogen atoms, H4 and H5, and the B atom in [$BF_4$] are available in the Supporting Information Figures S3 and S4. SDFs were also analyzed for [BMIM][$BF_4$] using an isosurface value of 7.50 particles/$nm^3$ for the anion region (colored in pink in Figure 7). Better agreement was found between the AIMD and OPLS-VSIL derived SDFs as compared to 0.8*OPLS-2009IL that lacked the "in-plane" hydrogen bond interaction. Overall, the cation-anion [BMIM][$BF_4$] solvent structure interactions computed using AIMD simulations were reasonably reproduced using both OPLS-based FFs, but greater structural accuracy was achieved by employing the OPLS-VSIL (Figures 6 and 7, and Table 2).

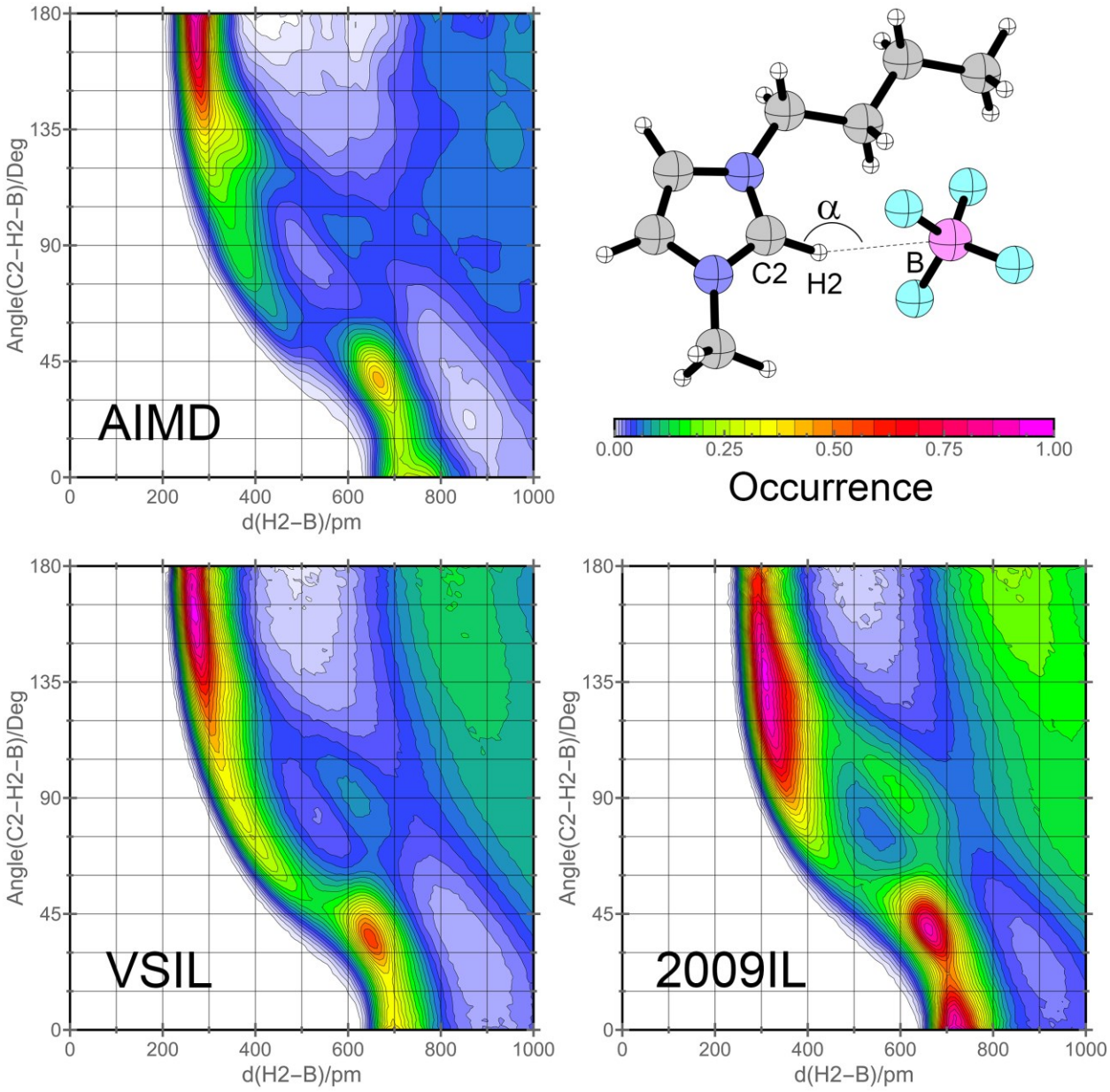


**Figure 6.** Combined distribution functions (CDFs) for the ionic liquid [BMIM][$BF_4$] from the AIMD, OPLS-VSIL, and OPLS-2009IL simulations. Illustrations are given of the plotted angle α versus the distance *d* between the H2 and B atoms. The CDF plot is given with a relative intensity color for the occurrence of the hydrogen bonding interaction.

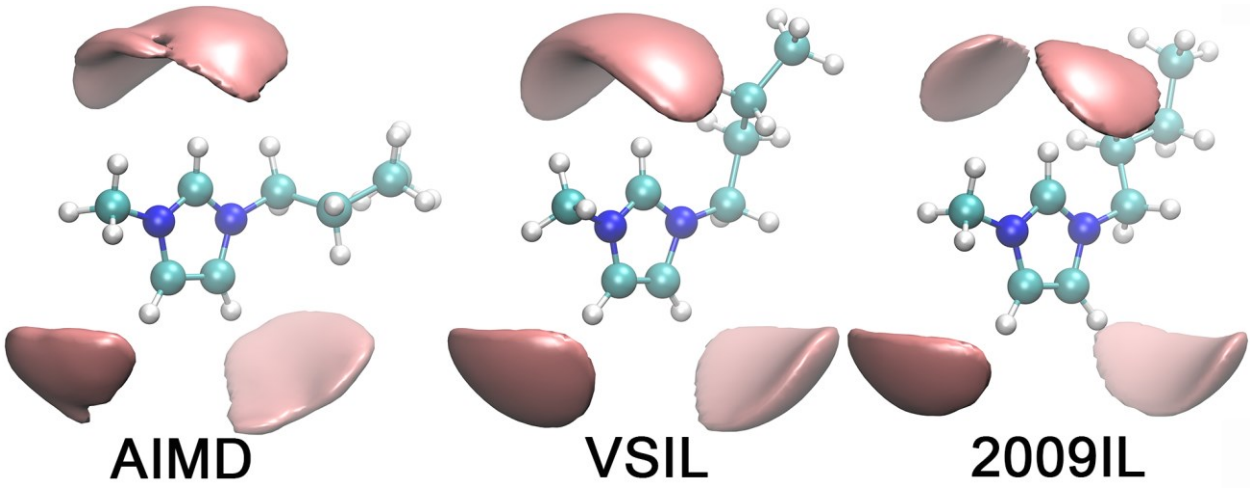


**Figure 7.** Spatial distribution function of the [$BF_4$] anion (pink color) around the [BMIM] cation in the ionic liquid simulation using AIMD, OPLS-VSIL, and OPLS-2009IL simulations.

In terms of cation-cation interactions, two-dimensional NOESY NMR experiments have examined $\pi^+$-$\pi^+$ cation-cation distances in [BMIM][$BF_4$] and their values suggest that the aromatic rings associate as sandwich and T-shaped assemblies.[85] Similar molecular arrangements have also been reported for [BMIM][$PF_6$] using X-ray reflectivity.[86] Interestingly, the AIMD simulation here emphasized the particular location of $d$ = 350-400 pm and α = 165-180° (shown in red in Figure 8) which corresponds to the parallel $\pi^+$-$\pi^+$ stacking orientation. The OPLS FFs sampled the configurational space more widely. For example, 0.8*OPLS-2009IL emphasized $\pi^+$-$\pi^+$ stacking orientations located at distances near 400 and 600 pm and a T-shaped assembly at 800-900 pm with an angle around 90°. However, similar to the [BMIM][$PF_6$] simulations, the OPLS-VSIL favored more of a slipped $\pi^+$-$\pi^+$ stacking orientation with a $d$ near 600 pm and α = 135-180° (or 0-45°).

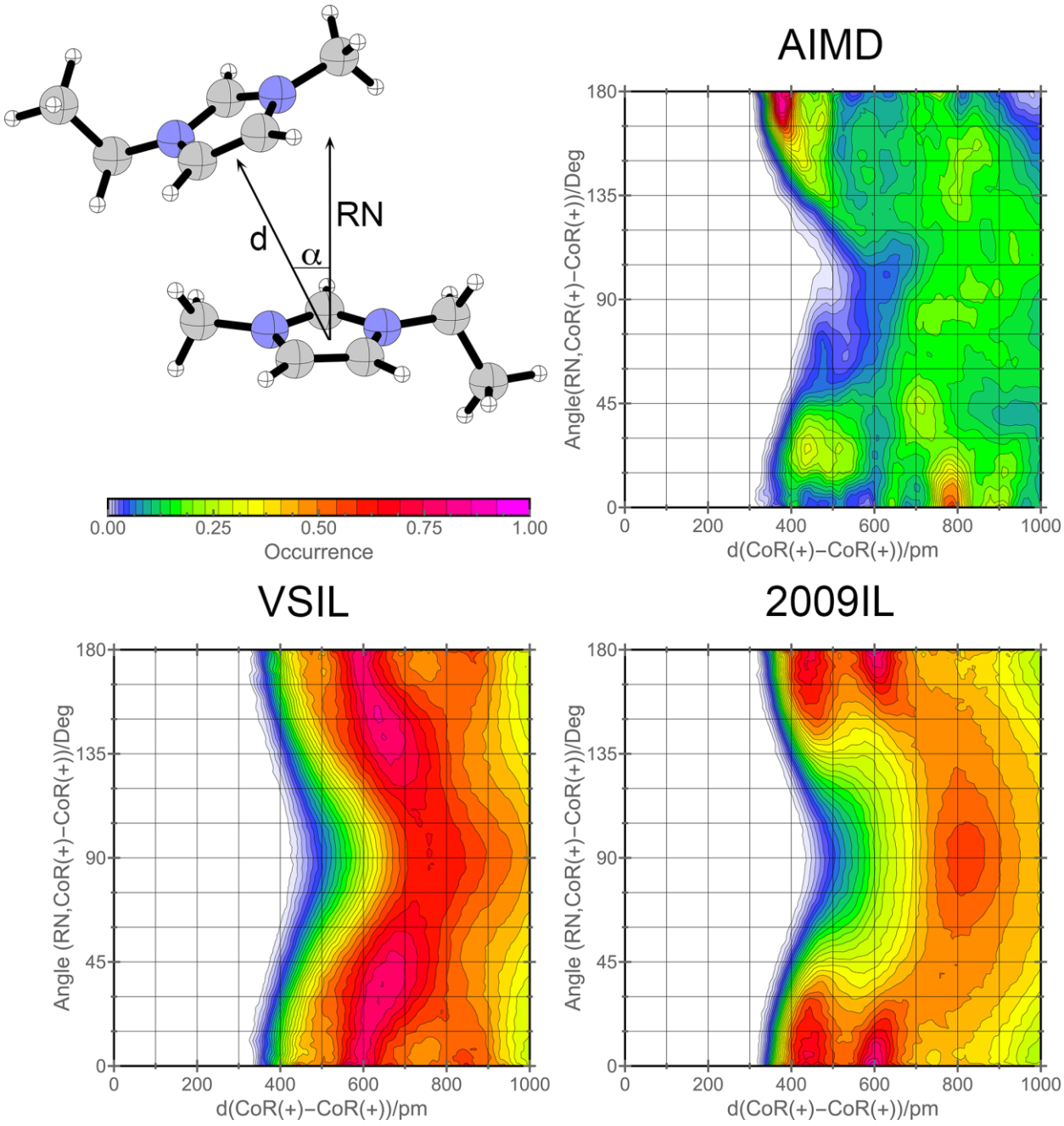


**Figure 8.** Combined distribution functions (CDFs) for the ionic liquid [BMIM][$BF_4$] from the OPLS-2009IL, OPLS-VSIL, and AIMD simulations. Illustrations are given of the plotted angle α versus the distance *d* for the center of the ring (CoR) interaction between two [BMIM]. The CDF plot is given with a relative intensity color for the CoR−CoR interactions. (Adapted with permission from *J. Phys. Chem. B* **2018**, *122*, 2962−2974. Copyright 2018 American Chemical Society).

**[BMIM][Cl].** The final IL combination studied here was [BMIM][Cl] and, like the previous ILs, the cation-anion interactions were analyzed using RDFs derived from the AIMD and OPLS FF simulations (Figures 9 and S3). The *g*(r) peak heights were generally similar for the AIMD and OPLS-VSIL methods, with the notable exception of the H4,5-Cl interaction that gave a substantially overestimated value of 5.8 versus 4.1 (Table 4). However, the H-Cl separation distances computed using the OPLS-VSIL were very accurate when compared to AIMD. Unfortunately, the 0.8*OPLS-2009IL did not fare as well with overestimated g(r) values and considerably large atom distances, e.g., H2-Cl of 271.7 pm compared to 228.3 pm from AIMD (Table 4). In principle, adjustment of the pairwise length scale ($\sigma_{ij}$) parameters of the nonbonded Lennard-Jones interaction between $Cl^-$ and [BMIM] could improve the agreement.[87]

Hunt and coworkers previously performed MD simulations on [EMIM][Cl] and [BMIM][Cl] ionic liquids and found that hydrogen bonding is highly angle dependent and temperature differences result in a variable, not static, network of hydrogen bonds.[88, 89] Accordingly, CDFs were used to further elaborate upon the solvent structure through monitoring the simulation distances and angles between the H2 atom of [BMIM] and $Cl^-$ (Figure 10). The AIMD simulations emphasized an intense interaction area at $d$ = 200-250 pm and α = 150-180° (colored in red in Figure 10). The OPLS-VSIL correctly reproduced the atom separation distance but gave a wider-angle preference of α = 125-180°. The 0.8*OPLS-2009IL gave an elongated distance of $d$ = 250-300 pm and a shifted α preference of 120-160°. Additional CDF plots between the [BMIM] ring hydrogen atoms, H4 and H5, and $Cl^-$ are available in the Supporting Information Figures S5 and S6.

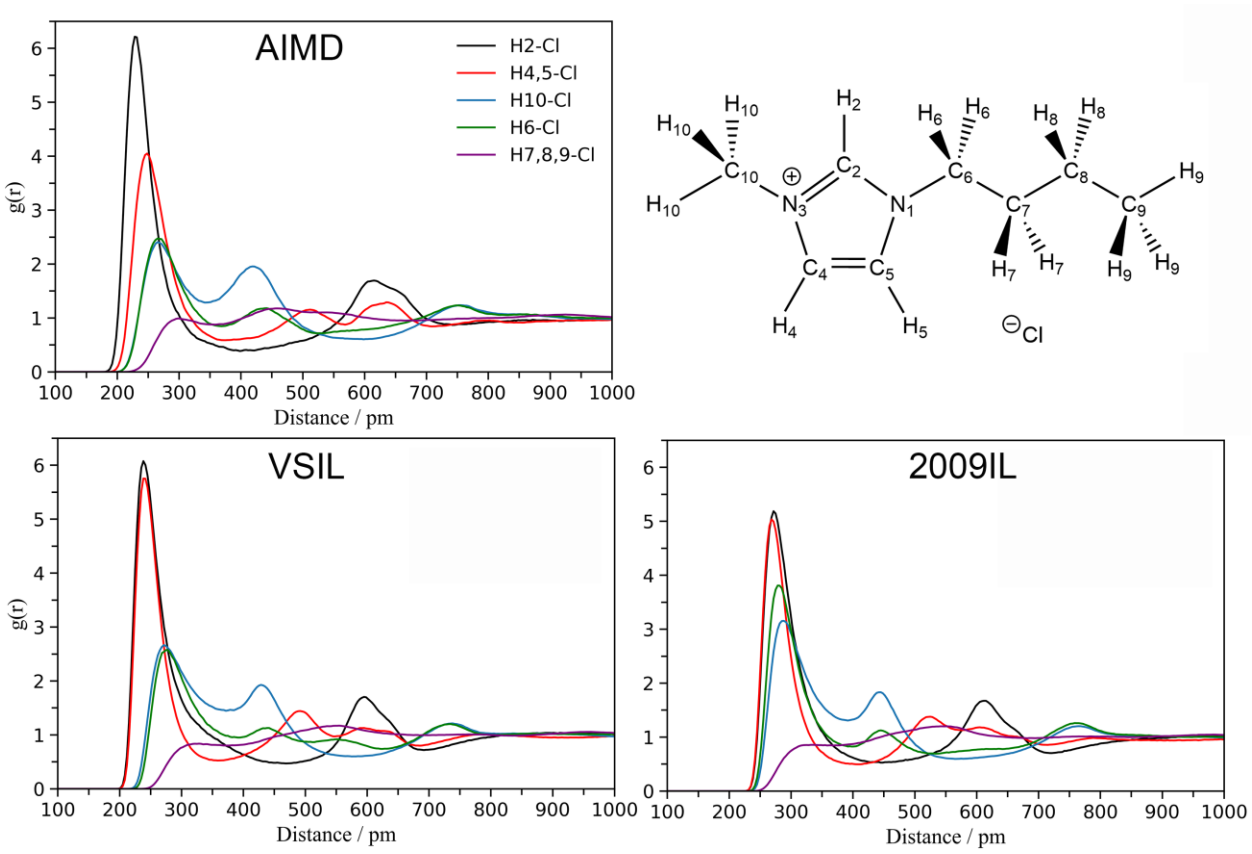


**Figure 9.** Computed radial distribution function plots between the hydrogen atoms of [BMIM] and chloride from the AIMD, OPLS-VSIL, and OPLS-2009IL simulations.

**Table 4.** Interaction Distances (pm) and *g*(r) from Radial Distribution Functions Computed using 0.8*OPLS-2009IL, OPLS-VSIL, and AIMD simulations for the Ionic Liquid [BMIM][Cl].

| | distance (pm) | | | *g*(r) | | |
|---|---|---|---|---|---|---|
| Atoms[a] | 2009IL | VSIL | AIMD | 2009IL | VSIL | AIMD |
| H2-Cl | 271.7 | 238.3 | 228.3 | 5.2 | 6.1 | 6.2 |
| H4,5-Cl | 268.3 | 238.3 | 248.3 | 5.0 | 5.8 | 4.1 |
| H10-Cl | 288.3 | 271.7 | 265.0 | 3.2 | 2.7 | 2.4 |
| H6-Cl | 278.3 | 275.0 | 265.0 | 3.8 | 2.6 | 2.5 |

[a]See Figure 9 for atom definitions.

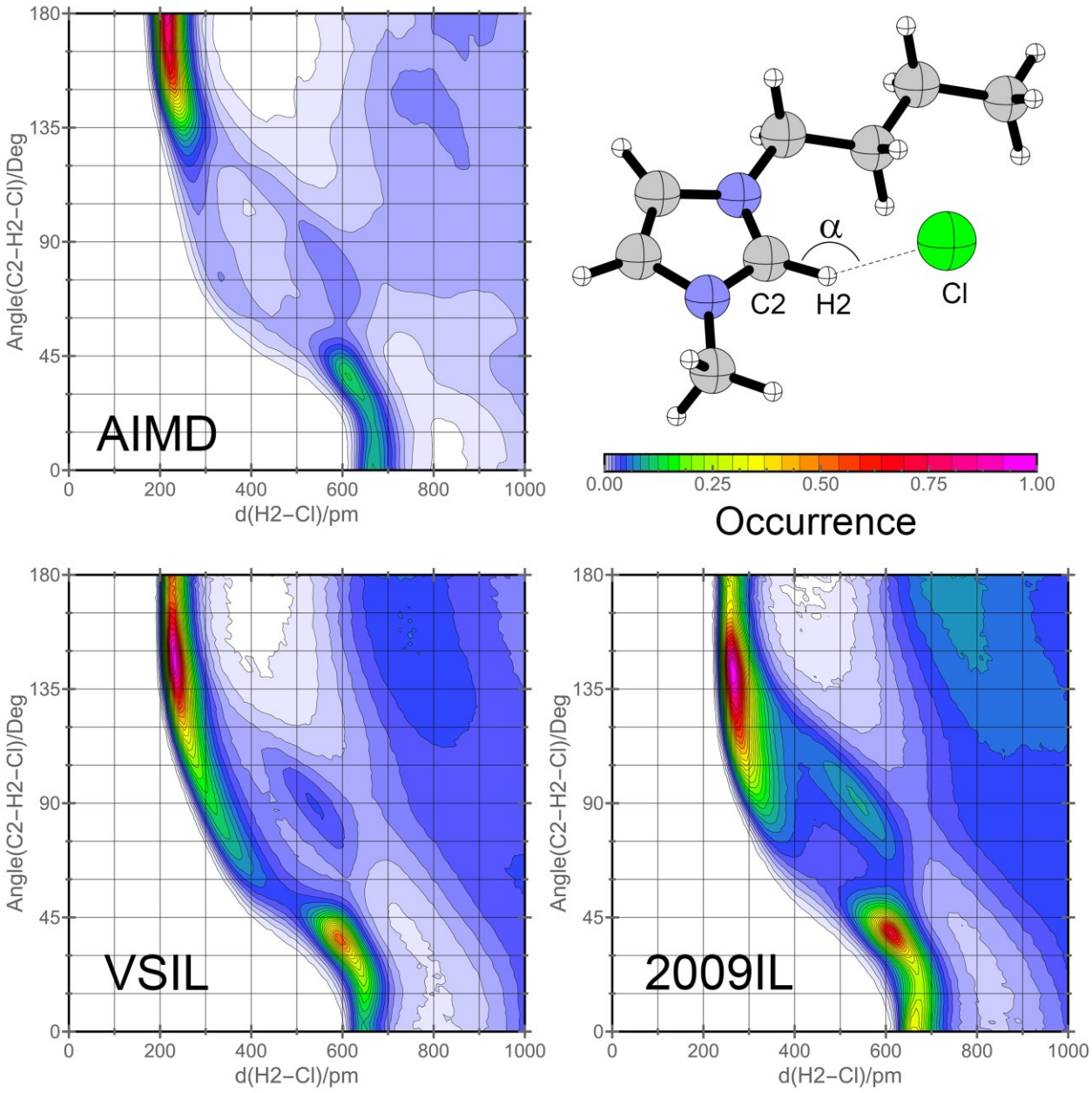


**Figure 10.** Combined distribution functions (CDFs) for the ionic liquid [BMIM][Cl] from the OPLS-2009IL, OPLS-VSIL, and AIMD simulations. Illustrations are given of the plotted angle α versus the distance *d* between H2 and $Cl^-$. The CDF plot is given with a relative intensity color for the occurrence of the hydrogen bonding interaction.

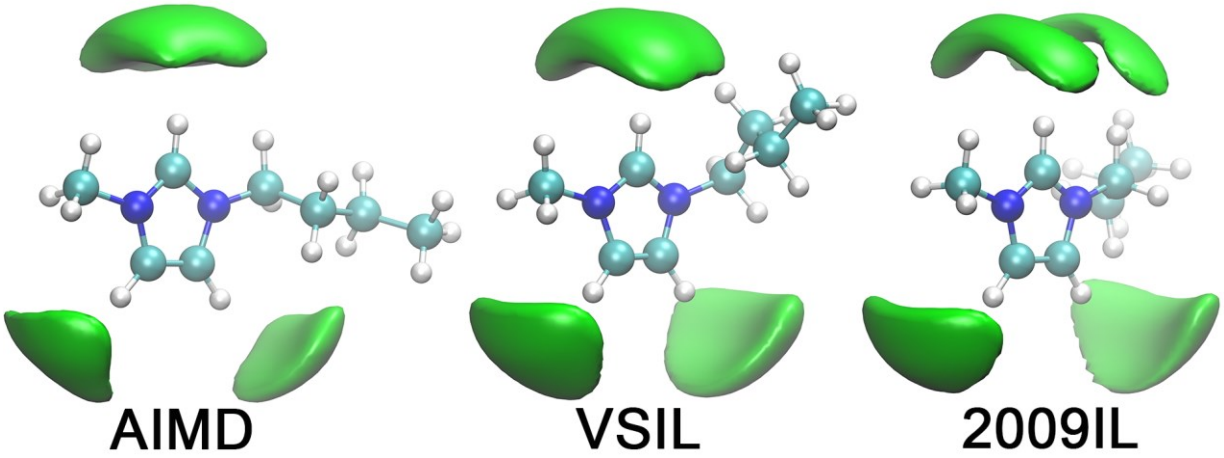


**Figure 11.** Spatial distribution function of the [Cl] anion (green color) around the [BMIM] cation in the ionic liquid simulation using OPLS-2009IL, OPLS-VSIL, and AIMD simulations.

The SDFs were computed for [BMIM][Cl] using an isosurface value of 11.0 particles/nm$^3$ for the anion region (colored in green in Figure 11) and were found to possess significant differences at the H2-Cl interaction when comparing the two OPLS FFs. For example, the 0.8*OPLS-2009IL FF found the [Cl] anions preferred to occupy the volume between the H2 atom on the ring and the H6 and H10 atoms bound to the alkyl side chains (Figure 11). This preference was not observed in either of the AIMD or OPLS-VSIL simulations. Gas-phase calculations using symmetry-adapted perturbation theory on a [BMIM][Cl] ion pair have reported on-top cation−anion interactions (i.e., above/below the ring) and in-plane hydrogen bonding be energetically equivalent.[75] However, the current solution-phase AIMD simulations found a preference for the in-plane interaction that may arise from preferential the $\pi^+$-$\pi^+$ stacking of the cations in solution. Examination of the CoRs interaction between two [BMIM] cations in Figure 12 found that AIMD favored the parallel $\pi^+$-$\pi^+$ stacked conformation with a $d_{\text{CoR-CoR}}$ of ~400 pm and $\alpha$ = 0-15°.

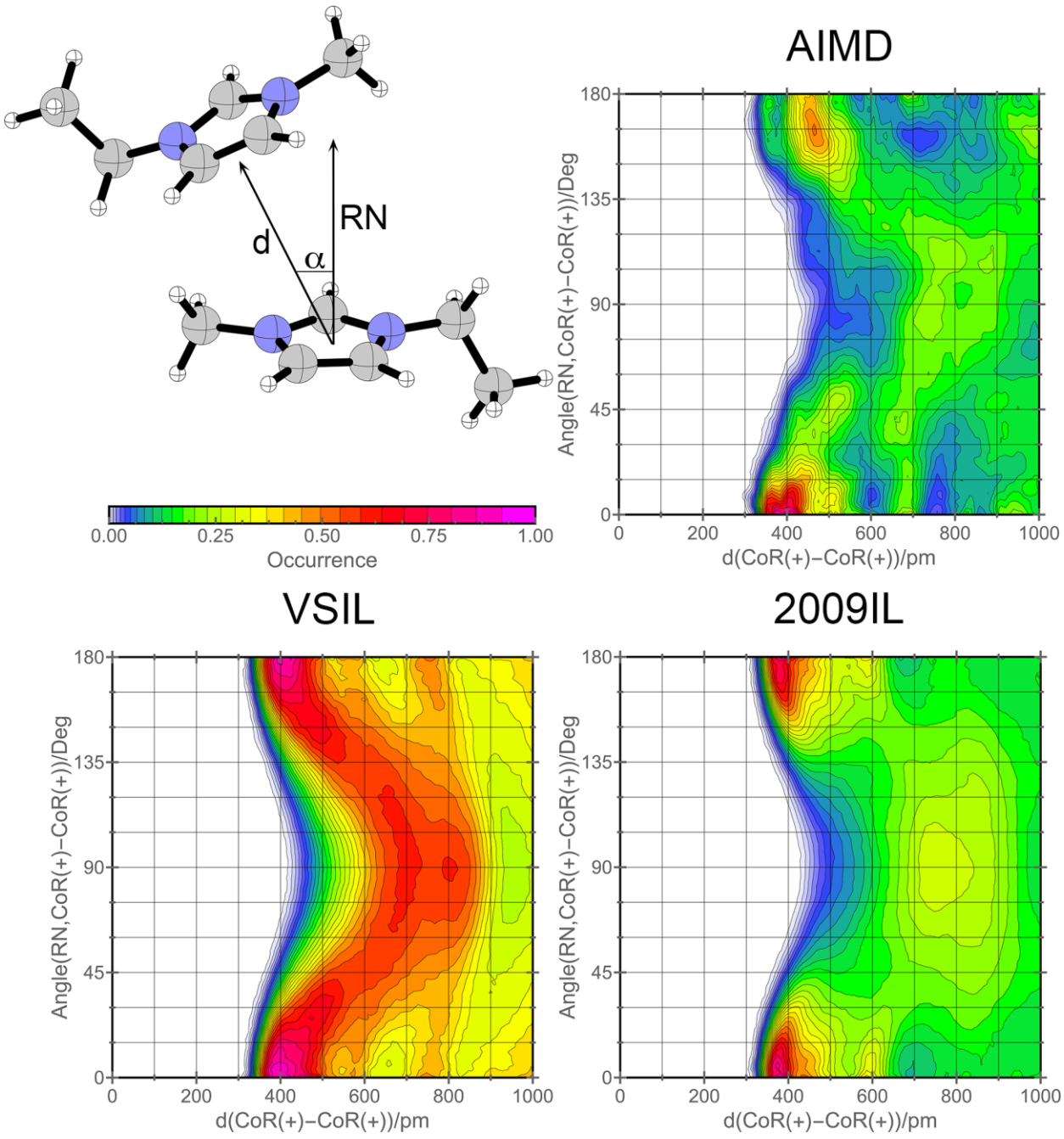


**Figure 12.** Combined distribution functions (CDFs) for the ionic liquid [BMIM][Cl] from the OPLS-2009IL, OPLS-VSIL, and AIMD simulations. Illustrations are given of the plotted angle α versus the distance *d* for the center of the ring (CoR) interaction between two [BMIM]. The CDF plot is given with a relative intensity color for the CoR−CoR interactions. (Adapted with permission from *J. Phys. Chem. B* **2018**, *122*, 2962−2974. Copyright 2018 American Chemical Society).

The 0.8*OPLS-2009IL did an excellent job of reproducing the $\pi^+$-$\pi^+$ interactions in the CDF analysis (Figure 12). The OPLS-VSIL also correctly reproduced the $\pi^+$-$\pi^+$ stacking between the BMIM rings at an approximate distance and angle of 400 pm and 0°/180°, respectively, but it also strongly emphasized the occurrence of the T-shape assembly.

## Conclusions

To summarize, AIMD simulations have been carried out on three imidazolium-based ionic liquids, [BMIM][$PF_6$], [BMIM][$BF_4$], and [BMIM][Cl], as a detailed investigation of their microscopic intermolecular solvent organization. Two unique ionic liquid force fields, i.e., the ±0.8 charge-scaled OPLS-2009IL and OPLS-VSIL, were examined for their ability to reproduce the QM-derived solvent structure. Both FFs provided a satisfactory reproduction of the AIMD-computed cation-anion interactions from analysis of radial, spatial, and combined distribution plots of the distances and angles between BMIM and the respective anion of each IL. In terms of cation-cation interactions, both OPLS-based FFs appropriately sampled the aromatic rings associated as $\pi^+$-$\pi^+$ sandwiches and T-shaped assemblies as expected from the AIMD simulations and reported in crystal structures. Despite the overall successful reproduction by the FFs, there were some discrepancies, particularly for the 0.8*OPLS-2009IL as it predicted longer cation-anion interaction distances and overemphasized the "on-top" ion-ion interaction for [BMIM][$PF_6$] and [BMIM][$BF_4$]. Overall, greater structural accuracy and absolute quantitative agreement with AIMD was achieved by employing the OPLS-VSIL. All ionic liquid force field parameters can be downloaded at https://github.com/orlandoacevedo/IL.

**Acknowledgement.** Gratitude is expressed to the National Science Foundation (CHE-2102038) for support of this research.

S**upporting Information Available:** Combined distribution functions between the [BMIM] H4 and H5 atoms and the P, B, and Cl atoms from the [$PF_6$], [$BF_4$], and [Cl] anions, respectively; radial distribution functions grouped according to unique atom pairs; examples of ion clusters for [BMIM][$PF_6$] simulations; and center-of-mass based radial distribution functions; The Supporting Information is available free of charge on the ACS Publications website at http://pubs.acs.org.

**References**


1. Gao, N.; He, Y.; Tao, X.; Xu, X.-Q.; Wu, X.; Wang, Y., Crystal-confined freestanding ionic liquids for reconfigurable and repairable electronics. *Nature Commun.* **2019,** *10*, 547.
2. Berthod, A.; Ruiz-Ángel, M. J.; Carda-Broch, S., Recent advances on ionic liquid uses in separation techniques. *J. Chromatogr. A* **2018,** *1559*, 2-16.
3. Watanabe, M.; Thomas, M. L.; Zhang, S.; Ueno, K.; Yasuda, T.; Dokko, K., Application of Ionic Liquids to Energy Storage and Conversion Materials and Devices. *Chem. Rev.* **2017,** *117*, 7190–7239.
4. Egorova, K. S.; Gordeev, E. G.; Ananikov, V. P., Biological Activity of Ionic Liquids and Their Application in Pharmaceutics and Medicine. *Chem. Rev.* **2017,** *117*, 7132–7189.
5. Ventura, S. P. M.; Silva, F. A. e.; Quental, M. V.; Mondal, D.; Freire, M. G.; Coutinho, J. A. P., Ionic-Liquid-Mediated Extraction and Separation Processes for Bioactive Compounds: Past, Present, and Future Trends. *Chem. Rev.* **2017,** *117*, 6984–7052.
6. Ho, T. D.; Zhang, C.; Leandro W. Hantao; Anderson, J. L., Ionic Liquids in Analytical Chemistry: Fundamentals, Advances, and Perspectives. *Anal. Chem.* **2014,** *86*, 262−285.
7. Olivier-Bourbigou, H.; Magna, L.; Morvan, D., Ionic liquids and catalysis: Recent progress from knowledge to applications. *Appl. Catal., A* **2010,** *373*, 1-56.
8. Plechkova, N. V.; Seddon, K. R., Applications of ionic liquids in the chemical industry. *Chem. Soc. Rev.* **2008,** *37*, 123-150.
9. Freemantle, M., *An Introduction to Ionic Liquids*. RSC Publishing: Cambridge, UK, 2009.
10. Rogers, R. D.; Seddon, K. R., Ionic Liquids--Solvents of the Future. *Science* **2003,** *31*, 792-793.

11. Welton, T., Room-Temperature Ionic Liquids. Solvents for Synthesis and Catalysis. *Chem. Rev.* **1999,** *99*, 2071-2083.

12. Hallett, J. P.; Welton, T., Room-Temperature Ionic Liquids: Solvents for Synthesis and Catalysis. 2. *Chem. Rev.* **2011,** *111*, 3508–3576.

13. Hayes, R.; Warr, G. G.; Atkin, R., Structure and Nanostructure in Ionic Liquids. *Chem. Rev.* **2015,** *115*, 6357–6426.

14. Chen, S.; Zhang, S.; Liu, X.; Wang, J.; Wang, J.; Dong, K.; Sun, J.; Xu, B., Ionic liquid clusters: structure, formation mechanism, and effect on the behavior of ionic liquids. *Phys. Chem. Chem. Phys.* **2014,** *16*, 5893-5906.

15. Kirchner, B.; Blasius, J.; Alizadeh, V.; Gansäuer, A.; Hollóczki, O., Chemistry Dissolved in Ionic Liquids. A Theoretical Perspective. *J. Phys. Chem. B* **2022,** *126*, 766–777.

16. Velez, C.; Acevedo, O., Simulation of Deep Eutectic Solvents: Progress to Promises. *WIREs Comput. Mol. Sci.* **2022**, e1598.

17. Nordness, O.; Brennecke, J. F., Ion Dissociation in Ionic Liquids and Ionic Liquid Solutions. *Chem. Rev.* **2020,** *120*, 12873–12902.

18. Izgorodina, E. I.; Seeger, Z. L.; Scarborough, D. L. A.; Tan, S. Y. S., Quantum Chemical Methods for the Prediction of Energetic, Physical, and Spectroscopic Properties of Ionic Liquids. *Chem. Rev.* **2017,** *117*, 6696–6754.

19. Dong, K.; Liu, X.; Dong, H.; Zhang, X.; Zhang, S., Multiscale Studies on Ionic Liquids. *Chem. Rev.* **2017,** *117*, 6636–6695.

20. Amarasekara, A. S., Acidic Ionic Liquids. *Chem. Rev.* **2016,** *116*, 6133–6183.

21. Zahn, S.; Brehm, M.; Brüssel, M.; Hollóczki, O.; Kohagen, M.; Lehmann, S.; Malberg, F.; Pensado, A. S.; Schöppke, M.; Weber, H.; Kirchner, B., Understanding ionic liquids from theoretical methods. *J. Mol. Liq.* **2014,** *192*, 71-76.

22. Wendler, K.; Dommert, F.; Zhao, Y. Y.; Berger, R.; Holmb, C.; Site, L. D., Ionic liquids studied across different scales: A computational perspective. *Faraday Discuss.* **2012,** *154*, 111-132.

23. Zahn, S.; Kirchner, B., Uncovering molecular secrets of ionic liquids. *Chem. Modell.* **2012,** *9*, 1-24.

24. Brela, M. Z.; Kubisiak, P.; Eilmes, A., Understanding the Structure of the Hydrogen Bond Network and Its Influence on Vibrational Spectra in a Prototypical Aprotic Ionic Liquid. *J. Phys. Chem. B* **2018,** *122*, 9527-9537.

25. Macchieraldo, R.; Esser, L.; Elfgen, R.; Voepel, P.; Zahn, S.; Smarsly, B. M.; Kirchner, B., Hydrophilic Ionic Liquid Mixtures of Weakly and Strongly Coordinating Anions with and without Water. *ACS Omega* **2018,** *3*, 8567-8582.

26. Shah, J. K., Ab Initio Molecular Dynamics Simulations of Ionic Liquids. *Ann. Rep. Comput. Chem.* **2018,** *14*, 95-122.

27. Byrne, A.; Krishnan, Y.; English, N. J., Ab Initio Molecular Dynamics Studies of the Effect of Solvation by Room-Temperature Ionic Liquids on the Vibrational Properties of a N719-Chromophore/Titania Interface. *J. Phys. Chem. C* **2018,** *122*, 26464–26471.

28. Thomas, M.; Sancho Sanz, I.; Holloczki, O.; Kirchner, B., Ab Initio Molecular Dynamics Simulations of Ionic Liquids. In *NIC Symposium 2016*, Binder, K.; Muller, M.; Kremer, M.; Schnurpfeil, A., Eds. 2016; Vol. 48, pp 117-124.

29. Weber, H.; Kirchner, B., Complex Structural and Dynamical Interplay of Cyano-Based Ionic Liquids. *J. Phys. Chem. B* **2016,** *120*, 2471−2483.

30. Zahn, S.; Cybik, R., Comparison of Four Ionic Liquid Force Fields to an Ab Initio Molecular Dynamics Simulation. *Am. J. Nano. Res. Appl.* **2014,** *2*, 19-26.

31. Del Pópolo, M. G.; Lynden-Bell, R. M.; Kohanoff, J., Ab Initio Molecular Dynamics Simulation of a Room Temperature Ionic Liquid. *J. Phys. Chem. B* **2005,** *109*, 5895–5902.

32. Tuckerman, M. E., Ab initio molecular dynamics: basic concepts, current trends and novel applications. *J. Phys.: Condens. Matter* **2002,** *14*, R1297–R1355.

33. Perlt, E.; Ray, P.; Hansen, A.; Malberg, F.; Grimme, S.; Kirchner, B., Finding the best density functional approximation to describe interaction energies and structures of ionic liquids in molecular dynamics studies. *J. Chem. Phys.* **2018,** *148*, 193835.

34. Grimme, S.; Antony, J.; Ehrlich, S.; Krieg, H., A Consistent and Accurate ab initio Parametrization of Density Functional Dispersion Correction (DFT-D) for the 94 Elements H-Pu. *J. Chem. Phys.* **2010,** *132*, 154104.

35. Grimme, S.; Hujo, W.; Kirchner, B., Performance of Dispersion-corrected Density Functional Theory for the Interactions in Ionic Liquids. *Phys. Chem. Chem. Phys.* **2012,** *14*, 4875−4883.

36. Zahn, S.; Kirchner, B., Validation of Dispersion-Corrected Density Functional Theory Approaches for Ionic Liquid Systems. *J. Phys. Chem. A* **2008,** *112*, 8430–8435.

37. Kirchner, B.; Seitsonen, A. P., Ionic Liquids from Car−Parrinello Simulations. 2. Structural Diffusion Leading to Large Anions in Chloraluminate Ionic Liquids. *Inorg. Chem.* **2007,** *46*, 2751-2754.

38. Spickermann, C.; Thar, J.; Lehmann, S. B. C.; Zahn, S.; Hunger, J.; Buchner, R.; Hunt, P. A.; Welton, T.; Kirchner, B., Why are ionic liquid ions mainly associated in water? A Car–Parrinello study of 1-ethyl-3-methyl-imidazolium chloride water mixture. *J. Chem. Phys.* **2008,** *129*, 104505.

39. Zahn, S.; Wendler, K.; Site, L. D.; Kirchner, B., Depolarization of water in protic ionic liquids. *Phys. Chem. Chem. Phys.* **2011,** *13*, 15083-15093.

40. Szabadi, A.; Elfgen, R.; Macchieraldo, R.; Kearns, F. L.; Woodcock, H. L.; Kirchner, B.; Schröder, C., Comparison between ab initio and polarizable molecular dynamics simulations of 1-butyl-3-methylimidazolium tetrafluoroborate and chloride in water. *J. Mol. Liq.* **2021,** *337*, 116521.

41. Salanne, M.; Siqueira, L. J. A.; Seitsonen, A. P.; Madden, P. A.; Kirchner, B., From molten salts to room temperature ionic liquids: Simulation studies on chloroaluminate systems. *Faraday Discuss.* **2012,** *154*, 171-188.

42. Campetella, M.; Macchiagodena, M.; Gontrani, L.; Kirchner, B., Effect of alkyl chain length in protic ionic liquids: an AIMD perspective. *Mol. Phys.* **2017,** *115*, 1582-1589.

43. Campetella, M.; Martino, D. C.; Scarpellini, E.; Gontrani, L., Low-Q peak in X-ray patterns of choline-phenylalanine and -homophenylalanine: A combined effect of chain and stacking. *Chem. Phys. Lett.* **2016,** *660*, 99-101.

44. Campetella, M.; Gontrani, L.; Bodo, E.; Ceccacci, F.; Marincola, F. C.; Caminiti, R., Conformational isomerisms and nano-aggregation in substituted alkylammonium nitrates ionic liquids: An x-ray and computational study of 2-methoxyethylammonium nitrate. *J. Phys. Chem.* **2013,** *138*, 184506.

45. Goloviznina, K.; Gong, Z.; Pádua, A. A. H., The CL&Pol polarizable force field for the simulation of ionic liquids and eutectic solvents. *WIREs Comput. Mol. Sci.* **2021**, e1572.

46. Goloviznina, K.; Gong, Z.; Gomes, M. F. C.; Pádua, A. A. H., Extension of the CL&Pol Polarizable Force Field to Electrolytes, Protic Ionic Liquids, and Deep Eutectic Solvents. *J. Chem. Theory Comput.* **2021,** *17*, 1606–1617.

47. Zhong, X.; Velez, C.; Acevedo, O., Partial Charges Optimized by Genetic Algorithms for Deep Eutectic Solvent Simulations. *J. Chem. Theory Comput.* **2021,** *17*, 3078-3087.

48. Bedrov, D.; Piquemal, J.-P.; Borodin, O.; MacKerell Jr., A. D.; Roux, B.; Schröder, C., Molecular Dynamics Simulations of Ionic Liquids and Electrolytes Using Polarizable Force Fields. *Chem. Rev.* **2019,** *119*, 7940–7995.

49. Doherty, B.; Acevedo, O., OPLS Force Field for Choline Chloride-Based Deep Eutectic Solvents. *J. Phys. Chem. B* **2018,** *122*, 9982-9993.

50. Kirchner, B.; Hollóczki, O.; Lopes, J. N. C.; Pádua, A. A. H., Multiresolution calculation of ionic liquids. *WIREs Comput. Mol. Sci.* **2015,** *5*, 202-214.

51. Salanne, M., Simulations of room temperature ionic liquids: from polarizable to coarse-grained force fields. *Phys. Chem. Chem. Phys.* **2015,** *17*, 14270-14279.

52. Dommert, F.; Wendler, K.; Berger, R.; Delle Site, L.; Holm, C., Force fields for studying the structure and dynamics of ionic liquids: a critical review of recent developments. *ChemPhysChem* **2012,** *13*, 1625-37.

53. Sambasivarao, S. V.; Acevedo, O., Development of OPLS-AA Force Field Parameters for 68 Unique Ionic Liquids. *J. Chem. Theory Comput.* **2009,** *5*, 1038-1050.

54. Doherty, B.; Zhong, X.; Gathiaka, S.; Li, B.; Acevedo, O., Revisiting OPLS Force Field Parameters for Ionic Liquid Simulations. *J. Chem. Theory Comput.* **2017,** *13*, 6131-6145.

55. Doherty, B.; Zhong, X.; Acevedo, O., Virtual Site OPLS Force Field for Imidazolium-Based Ionic Liquids. *J. Phys. Chem. B* **2018,** *122*, 2962-2974.

56. Velez, C.; Doherty, B.; Acevedo, O., Accurate Diels-Alder Energies and Endo Selectivity in Ionic Liquids using the OPLS-VSIL Force Field. *Int. J. Mol. Sci.* **2020,** *21*, 1190.

57. Hutter, J.; Iannuzzi, M.; Schiffmann, F.; VandeVondele, J., CP2k: Atomistic Simulations of Condensed Matter Systems. *WIREs Comput. Mol. Sci.* **2014,** *4*, 15-25.

58. VandeVondele, J.; Krack, M.; Mohamed, F.; Parrinello, M.; Chassaing, T.; Hutter, J., QUICKSTEP: Fast and Accurate Density Functional Calculations Using a Mixed Gaussian and Plane Waves Approach. *Comput. Phys. Commun.* **2005,** *167*, 103-128.

59. Saba, H.; Zhu, X.; Chen, Y.; Zhang, Y., Determination of physical properties for the mixtures of [BMIM]Cl with different organic solvents. *Chin. J. Chem. Eng.* **2015,** *23*, 804-811.

60. Huddleston, J. G.; Visser, A. E.; Reichert, W. M.; Willauer, H. D.; Broker, G. A.; Rogers, R. D., Characterization and comparison of hydrophilic and hydrophobic room temperature ionic liquids incorporating the imidazolium cation. *Green Chem.* **2001,** *3*, 156-164.

61. Martínez, L.; Andrade, R.; Birgin, E. G.; Martínez, J. M., Packmol: A package for building initial configurations for molecular dynamics simulations. *J. Comput. Chem.* **2009,** *30*, 2157-2164.

62. Zhang, Y.; Yang, W., Comment on "Generalized Gradient Approximation Made Simple". *Phys. Rev. Lett.* **1998,** *80*, 890.

63. Grimme, S.; Ehrlich, S.; Goerigk, L., Effect of the damping function in dispersion corrected density functional theory. *J. Comput. Chem.* **2011,** *32*, 1456−1465.

64. VandeVondele, J.; Hutter, J., Gaussian Basis Sets for Accurate Calculations on Molecular Systems in Gas and Condensed Phases. *J. Chem. Phys.* **2007,** *127*, 114105.

65. Goedecker, S.; Teter, M.; Hutter, J., Separable Dual-Space Gaussian Pseudopotentials. *Phys. Rev. B: Condens. Matter Mater. Phys.* **1996,** *54*, 1703−1710.

66. Hartwigsen, C.; Goedecker, S.; Hutter, J., Relativistic separable dual-space Gaussian pseudopotentials from H to Rn. *Phys. Rev. B* **1998,** *58*.

67. Krack, M., Pseudopotentials for H to Kr optimized for gradient-corrected exchange-correlation functionals. *Theor. Chem. Acc.* **2005,** *114*, 145-152.

68. Brehm, M.; Kirchner, B., TRAVIS - a free analyzer and visualizer for Monte Carlo and molecular dynamics trajectories. *J. Chem. Inf. Model.* **2011,** *51*, 2007-2023.

69. Jorgensen, W. L.; Maxwell, D. S.; Tirado-Rives, J., Development and Testing of the OPLS All-Atom Force Field on Conformational Energetics and Properties of Organic Liquids. *J. Am. Chem. Soc.* **1996,** *118*, 11225-11236.

70. Abraham, M. J.; Murtola, T.; Schulz, R.; Páll, S.; Smith, J. C.; Hess, B.; Lindahl, E., GROMACS: High performance molecular simulations through multi-level parallelism from laptops to supercomputers. *SoftwareX* **2015,** *1-2*, 19-25.

71. Bussi, G.; Donadio, D.; Parrinello, M., Canonical sampling through velocity rescaling. *J. Chem. Phys.* **2007,** *126*, 014101.

72. Kempter, V.; Kirchner, B., The role of hydrogen atoms in interactions involving imidazolium-based ionic liquids. *J. Mol. Struct.* **2010,** *972*, 22-34.

73. Peppel, T.; Roth, C.; Fumino, K.; Paschek, D.; Kockerling, M.; Ludwig, R., The Influence of Hydrogen-Bond Defects on the Properties of Ionic Liquids. *Angew. Chem. Int. Ed.* **2011,** *50*, 6661–6665.

74. Marekha, B. A.; Kaluginb, O. N.; Idrissi, A., Non-covalent interactions in ionic liquid ion pairs and ion pair dimers: a quantum chemical calculation analysis. *Phys. Chem. Chem. Phys.* **2015,** *17*, 16846-16857.

75. Izgorodina, E. I.; MacFarlane, D. R., Nature of Hydrogen Bonding in Charged Hydrogen-Bonded Complexes and Imidazolium-Based Ionic Liquids. *J. Phys. Chem. B* **2011,** *115*, 14659–14667.

76. Mondal, A.; Balasubramanian, S., Quantitative Prediction of Physical Properties of Imidazolium Based Room Temperature Ionic Liquids through Determination of Condensed Phase Site Charges: A Refined Force Field. *J. Phys. Chem. B* **2014,** *118*, 3409-3422.

77. Marekha, B. A.; Koverga, V. A.; Chesneau, E.; Kalugin, O. N.; Takamuku, T.; Jedlovszky, P. l.; Idrissi, A., Local Structure in Terms of Nearest-Neighbor Approach in 1-Butyl-3-methylimidazolium-Based Ionic Liquids: MD Simulations. *J. Phys. Chem. B* **2016,** *120*, 5029-5041.

78. Geronimo, I.; Singh, N. J.; Kim, K. S., Nature of anion-templated π+–π+ interactions. *Phys. Chem. Chem. Phys.* **2011,** *13*, 11841-11845.

79. Seth, S. K.; Manna, P.; Singh, N. J.; Mitra, M.; Jana, A. D.; Das, A.; Choudhury, S. R.; Kar, T.; Mukhopadhyay, S.; Kim, K. S., Molecular architecture using novel types of non-covalent π-interactions involving aromatic neutrals, aromatic cations and π-anions. *CrystEngComm* **2013,** *15*, 1285-1288.

80. Wilkes, J. S.; Zaworotko, M. J., Air and water stable 1-ethyl-3-methylimidazolium based ionic liquids. *J. Chem. Soc., Chem. Commun.* **1992**, 965-967.

81. Gao, W.; Tian, Y.; Xuan, X., How the cation–cation π–π stacking occurs: A theoretical investigation into ionic clusters of imidazolium. *J. Mol. Graphics Modell.* **2015,** *60*, 118-123.

82. Matthews, R. P.; Welton, T.; Hunt, P. A., Hydrogen bonding and π–π interactions in imidazolium-chloride ionic liquid clusters. *Phys. Chem. Chem. Phys.* **2015,** *17*, 14437-14453.

83. Matthews, R. P.; Welton, T.; Hunt, P. A., Competitive pi interactions and hydrogen bonding within imidazolium ionic liquids. *Phys. Chem. Chem. Phys.* **2014,** *16*, 3238-3253.

84. Weber, H.; Hollóczki, O.; Pensado, A. S.; Kirchner, B., Side chain fluorination and anion effect on the structure of 1-butyl-3-methylimidazolium ionic liquids. *J. Chem. Phys.* **2013,** *139*, 084502.

85. Mele, A.; Romanò, G.; Giannone, M.; Ragg, E.; Fronza, G.; Raos, G.; Marcon, V., The Local Structure of Ionic Liquids: Cation-Cation NOE Interactions and Internuclear Distances in Neat [BMIM][BF4] and [BDMIM][BF4]. *Angew. Chem. Int. Ed.* **2006,** *45*, 1123–1126.

86. Sloutskin, E.; Ocko, B. M.; Tamam, L.; Kuzmenko, I.; Gog, T.; Deutsch, M., Surface Layering in Ionic Liquids: An X-ray Reflectivity Study. *J. Am. Chem. Soc.* **2005,** *127*, 7796-7804.

87. Dhabal, D.; Patra, T., Molecular simulation of osmometry in aqueous solutions of the BMIMCl ionic liquid: a potential route to force field parameterization of liquid mixtures. *Phys. Chem. Chem. Phys.* **2020,** *22*, 28325-28338.

88. Skarmoutsos, I.; Dellis, D.; Matthews, R. P.; Welton, T.; Hunt, P. A., Hydrogen Bonding in 1-Butyl- and 1-Ethyl-3-methylimidazolium Chloride Ionic Liquids. *J. Phys. Chem. B* **2012,** *116*, 4921-4933.

89. Skarmoutsos, I.; Welton, T.; Hunt, P. A., The importance of timescale for hydrogen bonding in imidazolium chloride ionic liquids. *Phys. Chem. Chem. Phys.* **2014,** *16*, 3675-85.

**TOC Graphic**